

On the capacity of wireless systems employing OFDM-based spatial multiplexing*

Helmut Bölcskei¹⁾, David Gesbert²⁾, and Arogyaswami J. Paulraj²⁾

¹⁾ Information Systems Laboratory, Stanford University
Packard 223, 350 Serra Mall, Stanford, CA 94305-9510

Phone: (650)-724-3640, Fax: (650)-723-8473, email: bolcskei@rascals.stanford.edu
(on leave from the Dept. of Communications, Vienna University of Technology)

²⁾ Gigabit Wireless Inc., 1916B Old Middlefield Way, Mountain View, CA 94043
(on part-time leave from Information Systems Laboratory, Stanford University, Stanford, CA)

Correspondence should be addressed to H. Bölcskei

Abstract—We compute the capacity of wireless Orthogonal Frequency Division Multiplexing (OFDM)-based spatial multiplexing systems in delay spread environments. Introducing an abstract model to characterize the statistical properties of the space-time channel, we provide Monte-Carlo methods for estimating the capacity cumulative distribution function, expected capacity, and outage capacity of the OFDM-based spatial multiplexing system for the case where the channel is unknown at the transmitter and perfectly known at the receiver. We provide bounds on capacity, and we study the influence of physical parameters such as the amount of delay spread, angles of arrival, scattering radius, and line-of-sight component, and system parameters such as the number of antennas and antenna spacing on capacity. Applying our methods to spatial versions of the standard channels taken from the GSM recommendations allows us to make statements about achievable data rates of OFDM-based spatial multiplexing systems in practical broadband propagation environments.

Keywords: Smart antennas, Orthogonal frequency division multiplexing (OFDM), channel capacity, channel modeling.

*Submitted to *IEEE Trans. Communications*, Oct. 1999. This work was supported in part by FWF-grant J1629-TEC. Part of this paper will be submitted to IEEE ICASSP-00, Istanbul, Turkey, June 2000.

1 Introduction and Outline

The use of multiple antennas at both the base transceiver station (BTS) and the subscriber unit (SU) in a wireless system has recently been shown to have the potential of achieving extraordinary bit rates [1, 2, 3, 4]. The corresponding technology is known as spatial multiplexing [1] or BLAST [2, 5] and allows an increase in bit rate in a wireless radio link without additional power or bandwidth consumption. So far, most of the research in this context has focused on the narrowband flat-fading channel. Extensive investigations on the capacity of narrowband flat-fading (deterministic and stochastic) multi-antenna channels (assuming different levels of channel state information at the transmitter and the receiver) can be found in [2, 3, 5, 6, 7].

Contributions. In this paper, we compute the capacity of Orthogonal Frequency Division Multiplexing (OFDM)-based spatial multiplexing systems [1, 4, 8] employing blind transmission¹ in realistic broadband propagation environments with significant delay spread. Based on spatial channel models proposed in [9, 10, 11] and the space-time channel model suggested in [12, 9], we introduce a space-time channel model appropriate for OFDM-based spatial multiplexing in delay spread environments. Using this model, we then devise a Monte-Carlo method for estimating the capacity cumulative distribution function (cdf), expected capacity, and outage capacity of the spatial multiplexing system, and we provide bounds on capacity. Our channel model reveals the influence of physical parameters such as amount of delay spread, angles of arrival, scattering radius, path attenuations, and line-of-sight (LOS) component as well as system parameters such as the number of antennas and antenna spacing on capacity. We apply our Monte-Carlo method to study the impact of these parameters on capacity. Finally, we estimate the expected capacity, outage capacity, and capacity cdf of spatial versions of the *typical urban* (TU), and *hilly terrain* (HT) channels proposed in the GSM recommendations.

Relation to previous work. Our channel model builds on the research reported in [9, 10, 11, 12]. In particular, it is an extension of the space-time channel model proposed in [12, 9] to the case of multiple antennas at both the BTS and the SU.

The capacity of *deterministic multiple-input multiple-output (MIMO) channels* with memory and full channel knowledge at the transmitter and the receiver was derived in [13]. In [14] the capacity of *deterministic two-user multiaccess channels* with intersymbol-interference (ISI) is computed. Using a *parametric channel model* in which each path is described by an angle of departure, an angle of arrival,

¹By blind transmission, we mean that the channel is unknown at the transmitter and known at the receiver.

a (complex) path gain, and a path delay, the capacity of the corresponding deterministic MIMO delay spread channel (full channel knowledge at the transmitter and the receiver) has been provided in [4]. Using the same parametric channel model and defining the underlying path parameters as random variables a stochastic parametric channel model is established in [8], and an expression for the expected capacity is provided for the cases where the channel is either known at the receiver only or known at both the transmitter and the receiver. The channel model used in [4, 8] does not capture the effects of spatial fading correlation, diffuse scattering, and scattering radius on capacity and is therefore fundamentally different from the space-time channel model used in this paper. Furthermore, in the channel model used in [4, 8] each path can only be a rank 1 contributor to capacity², whereas in our model the rank depends on physically meaningful parameters such as angles of arrival, angular spread, and antenna spacing. As a consequence, we find that our space-time channel model is more flexible and generally also predicts higher capacities than the one used in [4, 8] (see Simulation Example 3).

The use of OFDM in the context of spatial multiplexing or BLAST has been proposed previously in [4, 8, 15, 16]. However, it appears that no capacity computation of an OFDM-based spatial multiplexing system using the physically motivated stochastic space-time channel model provided in this paper has been performed so far. For the single-carrier and narrowband flat-fading case, the impact of spatial fading correlation and antenna array geometry on capacity has been studied in [7]. To the best of our knowledge the impact of physical parameters (angles of arrival, scattering radius, and LOS-component) and system parameters (number of antennas and antenna spacing) on capacity in the delay spread case has not been studied in the literature so far.

Organization of the paper. The rest of this paper is organized as follows. In Section 2, we introduce the space-time channel model used in our subsequent investigations. In Section 3, OFDM-based spatial multiplexing is briefly described. In Section 4, we derive an expression for the capacity distribution of OFDM-based spatial multiplexing systems for blind transmission, and we provide bounds on capacity. In Section 5, we describe a Monte-Carlo based method for actually estimating the expected capacity, outage capacity, and the capacity cdf. We furthermore provide simulation results studying the influence of the propagation environment and system parameters on capacity, and we compute the capacity of spatial versions of standard channels taken from the GSM recommendations. Finally, Section 6 provides our conclusions and some future research directions.

²This statement will be made more clear in Sec. 2.4.

2 Space-Time Channel Model

In this section, we shall introduce a model for stochastic space-time delay spread channels based on a physical description of the propagation environment. We first state our general assumptions, and then consider the uplink and downlink separately.

2.1 General Assumptions

Propagation Scenario. We assume that the SU is surrounded by local scatterers so that fading at the SU-antennas is spatially uncorrelated. The BTS, however, is high enough so that it is unobstructed and no local scattering occurs. Therefore, spatial fading at the BTS will be correlated. It is well known that this spatial fading correlation will be governed by the BTS antenna spacing and the angle spread at the BTS array [17]. Our model does incorporate the power delay profile of the channel, but neglects shadowing. These assumptions on the propagation scenario are typical for cellular suburban deployments [17], where the BTS is on a tower or on the roof of a building and the terminal is on the street level and experiences the effect of local scattering.

In the following M_B, M_S, M_R and M_T denote the number of antennas at the BTS, SU, receiver, and transmitter, respectively. Clearly, in the uplink $M_R = M_B, M_T = M_S$ and in the downlink $M_R = M_S$ and $M_T = M_B$.

Channel. Following [12, 9] the delay spread can be modeled by assuming that there are L significant scatterer clusters (see Fig. 1), and that each of the paths emanating from within the same scatterer cluster experiences the same delay, i.e., the delay equals τ_l for all the paths originating from the l -th cluster ($l = 0, 1, \dots, L - 1$). In practice, local scatterers in the cluster introduce micro delay variations, which will, however, be neglected in our model. With $\mathbf{x}(t)$ denoting the $M_T \times 1$ transmitted signal vector and $\mathbf{y}(t)$ the $M_R \times 1$ received signal vector, respectively, we can therefore write

$$\mathbf{y}(t) = \sum_{l=0}^{L-1} \mathbf{H}_l \mathbf{x}(t - \tau_l)$$

with the $M_R \times M_T$ complex-valued random matrices \mathbf{H}_l denoting the l -th tap of the stochastic matrix-valued channel impulse response. Throughout this paper we assume that the elements of the \mathbf{H}_l are (possibly correlated) circularly symmetric complex gaussian random variables³. Each scatterer cluster has a mean angle of arrival at the BTS $\bar{\theta}_l$ (derived from the position of the scatterer

³A circularly symmetric complex gaussian random variable is a random variable $z = (x + jy) \sim \mathcal{CN}(0, \sigma^2)$, where x and y are i.i.d. $\mathcal{N}(0, \sigma^2/2)$.

cluster), an angular spread δ_l (proportional to the scattering radius of the cluster), and a (complex) path gain β_l (derived from the power delay profile of the channel). We furthermore assume that the *scatterer clusters are uncorrelated*, i.e.,⁴

$$\mathcal{E} \left[\text{vec}\{\mathbf{H}_l - \mathcal{E}\{\mathbf{H}_l\}\} \text{vec}^H\{\mathbf{H}_{l'} - \mathcal{E}\{\mathbf{H}_{l'}\}\} \right] = \mathbf{0}_{M_R M_T} \quad \text{for } l \neq l', \quad (1)$$

where

$$\text{vec}\{\mathbf{H}_l\} = [\mathbf{h}_{l,0}^T \ \mathbf{h}_{l,1}^T \ \dots \ \mathbf{h}_{l,M_T-1}^T]^T$$

with $\mathbf{h}_{l,k} = [h_{l,k}^{(0)} \ h_{l,k}^{(1)} \ \dots \ h_{l,k}^{(M_R-1)}]^T$ denoting the k -th column of the matrix \mathbf{H}_l , and $\mathbf{0}_{M_R M_T}$ is the all zero matrix of size $M_R M_T \times M_R M_T$.

Array geometry. We assume a uniform linear array (ULA) at both the BTS and the SU with identical antenna elements. The relative antenna spacing is denoted as $\Delta = \frac{d}{\lambda}$, where d is the absolute antenna spacing and $\lambda = c/f_c$ is the wavelength of a narrowband signal with center frequency f_c .

Fading statistics. We shall next consider two alternative characterizations of the spatial fading correlation at the BTS. These characterizations differ in that they assume different statistics of the angles of arrival, namely a gaussian distribution and a uniform distribution. Common to both models, however, is the assumption that the $\mathbf{h}_{l,k}$ ($l = 1, 2, \dots, L - 1$) have zero mean and that the $M_R \times M_R$ correlation matrix $\mathbf{R}_l = \mathcal{E}\{\mathbf{h}_{l,k} \mathbf{h}_{l,k}^H\}$ is independent of k , or equivalently the fading statistics are the same for all transmit antennas. In what follows, we allow a LOS-component in the channel by assuming that the vectors $\mathbf{h}_{0,k}$ ($k = 0, 1, \dots, M_T - 1$) corresponding to the path cluster containing the SU (see Fig. 1) potentially have nonzero mean, which in general depends on k . The spatial fading correlation matrix for that path cluster is given by $\mathbf{R}_0 = \mathcal{E}\{(\mathbf{h}_{0,k} - \mathcal{E}\{\mathbf{h}_{0,k}\})(\mathbf{h}_{0,k}^H - \mathcal{E}\{\mathbf{h}_{0,k}^H\})\}$. Defining⁵ $\rho_l(s\Delta, \bar{\theta}_l, \delta_l) = \mathcal{E}\{h_{l,k}^{(r)} h_{l,k}^{(r+s)*}\}$ for $l = 0, 1, \dots, L - 1$, $k = 0, 1, \dots, M_T - 1$ to be the fading correlation between two BTS antenna elements spaced $s\Delta$ wavelengths apart, the correlation matrix \mathbf{R}_l can be written as

$$[\mathbf{R}_l]_{m,n} = |\beta_l|^2 \rho_l((n - m)\Delta, \bar{\theta}_l, \delta_l). \quad (2)$$

Note that we have absorbed the power delay profile of the channel into the correlation matrices. Throughout this paper we will use $|\beta_0|^2 = 1$.

We shall next specialize (2) for a gaussian and for a uniform distribution of the angle of arrival at the BTS. Let us first assume that the angle of arrival for the l -th path cluster at the BTS is

⁴ \mathcal{E} denotes the expectation operator.

⁵For $l = 0$ this definition has to be modified taking into account that the $\mathbf{h}_{0,k}$ ($k = 0, 1, \dots, M_T - 1$) potentially have nonzero mean.

gaussian distributed around the mean angle of arrival $\bar{\theta}_l$, i.e., $\hat{\theta}_l \sim \mathcal{N}(0, \sigma_{\theta_l})$ with the actual angle of arrival given by $\theta_l = \bar{\theta}_l + \hat{\theta}_l$. The variance σ_{θ_l} is proportional to the angular spread δ_l and hence the scattering radius of the l -th path cluster. More specifically, one may set $\sigma_{\theta_l} = \arcsin(\frac{R_{s,l}}{R_l})$ [9], where $R_{s,l}$ is the scattering radius of the l -th path cluster and R_l is the distance between the BTS and the l -th cluster. For small angular spread, or equivalently small σ_{θ_l} , the correlation function is given by [9]

$$\rho_l(s\Delta, \bar{\theta}_l, \delta_l) \approx e^{-j2\pi s\Delta \cos(\bar{\theta}_l)} e^{-\frac{1}{2}(2\pi s\Delta \sin(\bar{\theta}_l)\sigma_{\theta_l})^2}.$$

Although this approximation is accurate only for small angular spread, it does provide the correct trend for large angular spread, namely uncorrelated spatial fading. Note that in the case $R_{s,l} = 0$ and hence $\sigma_{\theta_l} = 0$, the correlation matrix \mathbf{R}_l collapses to a rank-1 matrix and can be written as $\mathbf{R}_l = |\beta_l|^2 \mathbf{a}(\bar{\theta}_l) \mathbf{a}^H(\bar{\theta}_l)$ with the array response vector of the ULA given by

$$\mathbf{a}(\theta) = [1 \quad e^{j2\pi\Delta \cos(\theta)} \quad \dots \quad e^{j2\pi(M_R-1)\Delta \cos(\theta)}]^T. \quad (3)$$

Another model to describe the spatial fading correlation between BTS antennas proposed in [10, 11] assumes that the angles of arrival are uniformly distributed in $[\bar{\theta}_l - \delta_l, \bar{\theta}_l + \delta_l]$. The fading correlation between two BTS antennas spaced $s\Delta$ wavelengths apart has been derived in [10, 11] as

$$\begin{aligned} \rho_l(s\Delta, \bar{\theta}_l, \delta_l) &= J_0(2\pi s\Delta) + 2 \sum_{m=1}^{\infty} J_{2m}(2\pi s\Delta) \cos(2m(\bar{\theta}_l - \pi/2)) \frac{\sin(2m\delta_l)}{2m\delta_l} \\ &\quad + 2j \sum_{m=0}^{\infty} J_{2m+1}(2\pi s\Delta) \sin[(2m+1)(\bar{\theta}_l - \pi/2)] \frac{\sin((2m+1)\delta_l)}{(2m+1)\delta_l}, \end{aligned} \quad (4)$$

where the J_m are Bessel functions of the first kind. Note that just like in the gaussian case the rank of \mathbf{R}_l generated from (4) will be determined by the angular spread and the mean angle of arrival of the l -th path cluster. In the limiting case $\delta_l = 0$ the rank of the correlation matrix is 1.

2.2 Uplink Channel Model

Since fading is spatially uncorrelated at the SU and the fading statistics have been assumed to be the same for all SU antennas, in the uplink different columns of \mathbf{H}_l will be uncorrelated whereas different rows will be correlated. Factoring the $M_B \times M_B$ correlation matrix \mathbf{R}_l according to $\mathbf{R}_l = \mathbf{R}_l^{1/2} \mathbf{R}_l^{H/2}$, where $\mathbf{R}_l^{1/2}$ is of size $M_B \times M_B$, the $M_B \times M_S$ matrices \mathbf{H}_l can be written as

$$\mathbf{H}_0 = \sqrt{\gamma_0} \mathbf{H}_{\text{LOS}} + \sqrt{1 - \gamma_0} \mathbf{R}_0^{1/2} \mathbf{H}_{w,0} \quad (5)$$

$$\mathbf{H}_l = \mathbf{R}_l^{1/2} \mathbf{H}_{w,l}, \quad l = 1, 2, \dots, L - 1 \quad (6)$$

with the $\mathbf{H}_{w,l}$ being uncorrelated $M_B \times M_S$ matrices with i.i.d. $\mathcal{CN}(0, 1)$ entries, i.e.,

$$\mathcal{E} \left[\text{vec}\{\mathbf{H}_{w,l}\} \text{vec}^H\{\mathbf{H}_{w,l'}\} \right] = \mathbf{0}_{M_B M_S} \quad \text{for } l \neq l'. \quad (7)$$

The parameter $0 \leq \gamma_0 \leq 1$ denotes the strength of the LOS-component (Ricean factor), and

$$[\mathbf{H}_{\text{LOS}}]_{m,n} = e^{-j2\pi\Delta_{m,n}}$$

with $\Delta_{m,n}$ denoting the distance in wavelengths between the m -th receive and the n -th transmit antenna. For the sake of simplicity we assume that the antenna spacing at the BTS and the SU are the same. Note that if the distance between the BTS and the SU is large compared to the antenna spacing, the matrix \mathbf{H}_{LOS} will have low rank. In the LOS-case the path cluster containing the SU is Ricean fading rather than Rayleigh fading. More specifically, the matrix \mathbf{H}_0 has a nonzero mean, i.e., $\mathcal{E}\{\mathbf{H}_0\} = \sqrt{\gamma_0} \mathbf{H}_{\text{LOS}}$. We have decomposed the l -th tap of the stochastic matrix-valued channel impulse response into the product of a deterministic matrix $\mathbf{R}_l^{1/2}$ describing the spatial fading correlation and a stochastic matrix of i.i.d. complex gaussian random variables. This factorization will turn out very useful for the developments in Sec. 4.

2.3 Downlink Channel Model

In the downlink local scattering occurs at the receiver, which means that spatial fading is uncorrelated at the receiver antennas. Consequently, different rows of \mathbf{H}_l will be uncorrelated and different columns will be correlated. Employing the same assumptions on the scatterer statistics as in the uplink, the $M_S \times M_B$ matrices \mathbf{H}_l can be decomposed as

$$\begin{aligned} \mathbf{H}_0 &= \sqrt{\gamma_0} \mathbf{H}_{\text{LOS}} + \sqrt{1 - \gamma_0} \mathbf{H}_{w,0} \mathbf{R}_0^{T/2} \\ \mathbf{H}_l &= \mathbf{H}_{w,l} \mathbf{R}_l^{T/2}, \quad l = 1, 2, \dots, L - 1, \end{aligned} \quad (8)$$

where the $\mathbf{H}_{w,l}$ are $M_S \times M_B$ matrices of i.i.d. $\mathcal{CN}(0, 1)$ random variables.

2.4 Differences to the Parametric Channel Model

In the parametric channel model proposed in [4, 8] each tap \mathbf{H}_l can be written as

$$\mathbf{H}_l = \beta_l \mathbf{a}_R(\bar{\theta}_{R,l}) \mathbf{a}_D^T(\bar{\theta}_{D,l}), \quad l = 0, 1, \dots, L - 1,$$

where β_l denotes the (complex) path gain, $\bar{\theta}_{R,l}$ and $\bar{\theta}_{D,l}$ are the angle-of-arrival and angle-of-departure, respectively, of the l -th path, and $\mathbf{a}_R(\theta)$ and $\mathbf{a}_D(\theta)$ the $M_R \times 1$ and $M_T \times 1$ receive and transmit

array response vectors (cf. (3)), respectively. Note that \mathbf{H}_l will always have rank 1 even if the angles $\bar{\theta}_{R,l}$ and $\bar{\theta}_{D,l}$ and the path gain β_l are random variables. In our space-time channel model the rank of the matrices \mathbf{H}_l is controlled by the fading correlation at the BTS. If the angular spread of the l -th path cluster is large, \mathbf{H}_l will have full rank, whereas for small angular spread the rank of \mathbf{H}_l will decrease. This follows from (6) and (8) and the fact that the correlation matrix \mathbf{R}_l loses rank if the angular spread decreases. The space-time channel model proposed in this paper is therefore more flexible than the parametric channel model [4, 8] and seems to be a more adequate description of a real-world scattering environment. Loosely speaking, the rank of the matrix \mathbf{H}_l determines “how many spatial subchannels the l -th path sees”. As a consequence the capacity obtained using our channel model can be as low as the capacity predicted by the parametric channel model, but will in the presence of angle spread in general be significantly higher (see Simulation Example 3).

3 OFDM-based Spatial Multiplexing

In this section, we will briefly discuss the OFDM-based spatial multiplexing system under consideration and provide some preparation for Sec. 4.

Spatial Multiplexing. Spatial Multiplexing [1], also referred to as BLAST technology [2, 5] has the potential to dramatically increase the capacity of wireless radio links with no additional power or bandwidth consumption. The technology requires multiple antennas at the BTS and the SU and works as follows. In the transmitter the (possibly coded) information symbol stream is split up into independent substreams, which are then simultaneously sent from the M_T transmit antennas. Due to the presence of scattering objects (buildings, cars, hills, etc.) each signal undergoes multipath propagation, which provides each transmit antenna with a different spatial signature. In the receiver, signal processing is employed to combine the individual data streams and to decode them. Under certain conditions on the matrix channel (propagation environment) [2, 5, 4] the transmitted signals “effectively see $\min(M_T, M_R)$ spatial channels within the same bandwidth”, which leads to a significant increase in capacity as compared to single-antenna systems. The advantage of spatial multiplexing is that almost orthogonal signatures of the transmitted signals are obtained for free by the propagation channel. In contrast, in CDMA and TDMA systems orthogonal signatures are created in the transmitter at the expense of frequency or time spreading and hence reduced spectral efficiency.

Orthogonal Frequency Division Multiplexing. Orthogonal frequency division multiplexing

(OFDM) [18, 19, 20, 21] has become part of several telecommunications standards, for example satellite and terrestrial digital audio broadcasting (DAB), digital terrestrial TV broadcasting (DVB) [22], asymmetric digital subscriber line (ADSL) for high-bit-rate digital subscriber services on twisted-pair channels, and broadband indoor wireless systems [23]. One of the main reasons for using OFDM is the fact that it turns the frequency-selective fading channel into a set of independent parallel gaussian channels with frequency-flat fading, which makes equalization simple. In the context of multi-antenna systems, the use of OFDM is even more attractive since multi-channel equalization (which is in general computationally very expensive) is drastically simplified in that for each OFDM-tone only a constant matrix has to be inverted [4, 8].

OFDM-based Spatial Multiplexing. Let us assume that the delay spread of the matrix channel is L taps, i.e., the channel transfer matrix can be written as

$$\mathbf{H}(e^{j2\pi\theta}) = \sum_{l=0}^{L-1} \mathbf{H}_l e^{-j2\pi l\theta}$$

with the channel impulse response matrix taps \mathbf{H}_l . Note that now \mathbf{H}_l denotes the discrete-time channel impulse response obtained by sampling the continuous-time impulse response at a rate of $\frac{1}{W}$, where W is the bandwidth of the analog OFDM-signal. We assume that the OFDM system employs a cyclic prefix (CP) [19], which is a copy of the last part of the OFDM symbol prepended to the symbol. The CP acts as a guard space between consecutive OFDM symbols and avoids ISI if the channel impulse response length L is smaller than the length of the CP. Furthermore, if the channel does not change within one OFDM symbol, inter-carrier interference (ICI) will also be avoided. In the following, we shall assume that the length of the CP is L . Fig. 2 shows a baseband OFDM transceiver employing N subcarriers. The modulator applies an N -point IFFT to N data symbols and then prepends the CP of length L , so that the overall OFDM symbol length is given by $M = N + L$. In the receiver, the CP is first removed and then an FFT is applied. In an OFDM-based spatial multiplexing system the (possibly coded) data stream corresponding to the i -th antenna is first passed through an OFDM modulator and then transmitted from the i -th antenna. Note that this transmission takes place simultaneously from all M_T transmit antennas. In the receiver, the individual signals are passed through an OFDM demodulator, separated, and then decoded. Fig. 3 shows a schematic view of an OFDM-based spatial multiplexing system. As already mentioned above, in the single-antenna case, if the length of the CP is greater than or equal to the channel length, the frequency-selective fading channel decouples into a set of parallel gaussian frequency-flat fading channels with correlated channel attenuations [19]. In the multi-antenna case we have a similar

result. Organizing the transmitted data symbols into frequency vectors $\mathbf{c}_k = [c_k^{(0)} \ c_k^{(1)} \ \dots \ c_k^{(M_T-1)}]^T$ with $c_k^{(i)}$ denoting the data symbol transmitted from the i -th antenna on the k -th tone, it can be shown that

$$\hat{\mathbf{c}}_k = \mathbf{H}(e^{j2\pi\frac{k}{N}})\mathbf{c}_k + \mathbf{n}_k, \quad (9)$$

where $\hat{\mathbf{c}}_k$ denotes the reconstructed data vector for the k -th tone, and \mathbf{n}_k is additive white gaussian noise satisfying

$$\mathcal{E}\{\mathbf{n}_k\mathbf{n}_l^H\} = \sigma_n^2\mathbf{I}_{M_R}\delta[k-l], \quad (10)$$

where \mathbf{I}_{M_R} is the identity matrix of size M_R . From (9) it follows that equalization becomes very simple, since for each tone $k = 0, 1, \dots, N-1$ the inversion of a constant matrix is required only. We note that (9) has been reported for the parametric channel model (described in Sec. 2.4) in [4, 8]. The proof for the more general channel model employed in this paper is fairly straightforward and will therefore not be provided.

4 Capacity of OFDM-based Spatial Multiplexing Systems

In this section, we shall compute the capacity of an OFDM-based spatial multiplexing system using the space-time channel model introduced in Sec. 2. We note that since the channel is random its capacity will be a random variable. Furthermore, we emphasize that only in the limiting case where the number of tones in the OFDM system goes to infinity the capacity of the OFDM-based spatial multiplexing system approaches the exact capacity of the underlying space-time channel. This follows using a result established for single-input single-output deterministic ISI channels in [24]. A more detailed discussion of this observation, however, is beyond the scope of this paper.

4.1 Preparation

We start by stacking the vectors $\hat{\mathbf{c}}_k$, \mathbf{c}_k , and \mathbf{n}_k according to

$$\hat{\mathbf{c}} = [\hat{\mathbf{c}}_0^T \ \hat{\mathbf{c}}_1^T \ \dots \ \hat{\mathbf{c}}_{N-1}^T]^T, \quad \mathbf{c} = [\mathbf{c}_0^T \ \mathbf{c}_1^T \ \dots \ \mathbf{c}_{N-1}^T]^T, \quad \mathbf{n} = [\mathbf{n}_0^T \ \mathbf{n}_1^T \ \dots \ \mathbf{n}_{N-1}^T]^T,$$

where $\hat{\mathbf{c}}$ and \mathbf{n} are $M_R N \times 1$ vectors and \mathbf{c} is an $M_T N \times 1$ vector. Note that (10) implies that the noise vector \mathbf{n} is white, i.e.,

$$\mathcal{E}\{\mathbf{nn}^H\} = \sigma_n^2\mathbf{I}_{M_R N}.$$

We furthermore define the $NM_R \times NM_T$ block-diagonal matrix

$$\mathbf{H} = \text{diag}\{\mathbf{H}(e^{j2\pi\frac{k}{N}})\}_{k=0}^{N-1}.$$

With these definitions the input-output relation (9) can be rewritten as

$$\hat{\mathbf{c}} = \mathbf{H}\mathbf{c} + \mathbf{n}. \quad (11)$$

By stacking the individual frequency-domain subchannels we have thus converted the input-output relation of the $M_R \times M_T$ broadband channel to the input-output relation of an $NM_R \times NM_T$ narrow-band channel with block-diagonal transfer matrix. This result allows us to conveniently compute the capacity of the broadband channel. In the following, we will assume that there is no LOS-component and hence $\gamma_0 = 0$. The LOS-case will be treated separately in Sec. 4.4.

4.2 General Results on Capacity

In the following we assume that for each channel use an independent realization of the random channel impulse response matrices \mathbf{H}_l is drawn and that the channel remains constant within one channel use. Using (11) the capacity (in bps/Hz) of the OFDM-based spatial multiplexing system under an average transmitter power constraint is given by⁶ [25, 26]

$$C = \max_{\text{tr}(\mathbf{\Sigma}) \leq P} \frac{1}{N} \log \left[\det \left(\mathbf{I}_{NM_R N} + \frac{1}{\sigma_n^2} \mathbf{H}\mathbf{\Sigma}\mathbf{H}^H \right) \right], \quad (12)$$

where $\mathbf{\Sigma}$ is the covariance matrix of the gaussian input vector \mathbf{c} and P is the maximum overall transmit power. Note that the capacity is normalized by N , since N data symbols are transmitted in one OFDM symbol. The $NM_T \times NM_T$ matrix $\mathbf{\Sigma}$ is a block-diagonal matrix given by

$$\mathbf{\Sigma} = \text{diag}\{\mathbf{\Sigma}_k\}_{k=0}^{N-1},$$

where the $M_T \times M_T$ matrices $\mathbf{\Sigma}_k$ are the covariance matrices of the gaussian vectors \mathbf{c}_k , and as such determine the power allocation across the transmit antennas and across the OFDM tones. If the channel is known at the transmitter, the optimum power allocation is obtained by distributing the total available power according to the water-filling solution [4, 8, 25, 26, 3, 7]. Since we are considering blind transmission (i.e. the channel is not known at the transmitter), the optimum power distribution strategy is to allocate equal power to all the space-frequency subchannels [4, 8]. In what follows we

⁶Throughout the paper all logarithms are to the base 2.

therefore set $\mathbf{\Sigma}_k = \frac{P}{M_T N} \mathbf{I}_{M_T}$ ($k = 0, 1, \dots, N - 1$). It is easily verified that this choice results in $\text{tr}(\mathbf{\Sigma}) = P$. We note that for certain applications even if channel state information is available at the transmitter uniform power allocation might be preferred over space-frequency water-filling since its implementation is more simple.

With uniform power allocation the capacity is obtained from (12) as

$$C = \frac{1}{N} \log \left[\det \left(\mathbf{I}_{M_R N} + \rho \mathbf{H} \mathbf{H}^H \right) \right], \quad (13)$$

where $\rho = \frac{P}{M_T N \sigma_n^2}$. Next, since $\mathbf{H} \mathbf{H}^H$ is block-diagonal it follows that $\mathbf{I}_{M_R N} + \rho \mathbf{H} \mathbf{H}^H$ is block-diagonal as well, which using [27]

$$\det \left(\mathbf{I}_{M_R N} + \rho \mathbf{H} \mathbf{H}^H \right) = \prod_{k=0}^{N-1} \det \left(\mathbf{I}_{M_R} + \rho \mathbf{H} \left(e^{j2\pi \frac{k}{N}} \right) \mathbf{H}^H \left(e^{j2\pi \frac{k}{N}} \right) \right)$$

yields

$$C = \frac{1}{N} \sum_{k=0}^{N-1} \log \left[\det \left(\mathbf{I}_{M_R} + \rho \mathbf{H} \left(e^{j2\pi \frac{k}{N}} \right) \mathbf{H}^H \left(e^{j2\pi \frac{k}{N}} \right) \right) \right]. \quad (14)$$

The capacity of the delay spread channel is therefore equal to the sum of the capacities of the individual subchannels $\mathbf{H} \left(e^{j2\pi \frac{k}{N}} \right)$ divided by N .

4.3 Derivation of the Capacity Distribution

We shall next derive an expression for the capacity distribution of OFDM-based spatial multiplexing systems. For the sake of clarity of presentation, we shall consider the uplink and downlink separately, although the capacity distribution is the same in both cases. In the following the notation $x \sim y$ means that the distribution of the random variable x is equal to the distribution of the random variable y .

Uplink capacity. Using (5) and (6) with $\gamma_0 = 0$, we get

$$\mathbf{H} \left(e^{j2\pi \frac{k}{N}} \right) = \sum_{l=0}^{L-1} \mathbf{R}_l^{1/2} e^{-j2\pi \frac{k}{N} l} \mathbf{H}_{w,l} \quad (15)$$

with the independent $M_B \times M_S$ matrices $\mathbf{H}_{w,l}$ consisting of uncorrelated circularly symmetric complex gaussian random variables $\mathcal{CN}(0, 1)$. Now (15) can be rewritten as

$$\mathbf{H} \left(e^{j2\pi \frac{k}{N}} \right) = \left[\mathbf{R}_0^{1/2} \quad \mathbf{R}_1^{1/2} e^{-j2\pi \frac{k}{N}} \quad \dots \quad \mathbf{R}_{L-1}^{1/2} e^{-j2\pi \frac{k}{N} (L-1)} \right] \begin{bmatrix} \mathbf{H}_{w,0} \\ \mathbf{H}_{w,1} \\ \vdots \\ \mathbf{H}_{w,L-1} \end{bmatrix} = \mathbf{R}^{1/2} (\mathbf{W}_k \otimes \mathbf{I}_{M_B}) \mathbf{H},$$

where the following definitions have been used

$$\mathbf{R}^{1/2} = [\mathbf{R}_0^{1/2} \ \mathbf{R}_1^{1/2} \ \dots \ \mathbf{R}_{L-1}^{1/2}], \quad \mathbf{W}_k = \text{diag}\{e^{-j2\pi\frac{k}{N}l}\}_{l=0}^{L-1}, \quad \mathbf{H} = [\mathbf{H}_{w,0}^T \ \mathbf{H}_{w,1}^T \ \dots \ \mathbf{H}_{w,L-1}^T]^T$$

and \otimes stands for the Kronecker product. Consequently, the product $\mathbf{H}(e^{j2\pi\frac{k}{N}})\mathbf{H}^H(e^{j2\pi\frac{k}{N}})$ is given by

$$\mathbf{H}(e^{j2\pi\frac{k}{N}})\mathbf{H}^H(e^{j2\pi\frac{k}{N}}) = \mathbf{R}^{1/2}(\mathbf{W}_k \otimes \mathbf{I}_{M_B})\mathbf{H}\mathbf{H}^H(\mathbf{W}_k^H \otimes \mathbf{I}_{M_B})\mathbf{R}^{H/2}. \quad (16)$$

Further simplifications can be accomplished using the SVD of the $M_B \times M_B L$ matrices $\mathbf{R}^{1/2}(\mathbf{W}_k \otimes \mathbf{I}_{M_B})$ given by

$$\mathbf{R}^{1/2}(\mathbf{W}_k \otimes \mathbf{I}_{M_B}) = \mathbf{U}_k \mathbf{D}_k \mathbf{V}_k^H, \quad (17)$$

where \mathbf{U}_k is an $M_B \times M_B$ unitary matrix, \mathbf{V}_k is an $M_B L \times M_B L$ unitary matrix, and \mathbf{D}_k is an $M_B \times M_B L$ matrix given by

$$\mathbf{D}_k = [\mathbf{\Lambda}_k \ \underbrace{\mathbf{0}_{M_B} \ \dots \ \mathbf{0}_{M_B}}_{(L-1) \text{ times}}] \quad \text{with} \quad \mathbf{\Lambda}_k = \text{diag}\{\lambda_{k,l}\}_{l=0}^{M_B-1}. \quad (18)$$

Using (14),(16) and (17) we obtain the following distribution for uplink capacity

$$C \sim \frac{1}{N} \sum_{k=0}^{N-1} \log \left[\det \left(\mathbf{I}_{M_B} + \rho \mathbf{D}_k \mathbf{V}_k^H \mathbf{H}\mathbf{H}^H \mathbf{V}_k \mathbf{D}_k^H \right) \right],$$

where we have used the fact that $\det(\mathbf{I} + \mathbf{Q}\mathbf{H}\mathbf{Q}^H) = \det(\mathbf{I} + \mathbf{H})$ for unitary \mathbf{Q} . Next, noting that the unitarity of the matrices \mathbf{V}_k implies that [28]

$$\mathbf{V}_k^H \mathbf{H}\mathbf{H}^H \mathbf{V}_k \sim \mathbf{H}\mathbf{H}^H,$$

we get

$$C \sim \frac{1}{N} \sum_{k=0}^{N-1} \log \left[\det \left(\mathbf{I}_{M_B} + \rho \mathbf{D}_k \mathbf{H}\mathbf{H}^H \mathbf{D}_k^H \right) \right]. \quad (19)$$

Now, using (18), we obtain

$$\mathbf{D}_k \mathbf{H}\mathbf{H}^H \mathbf{D}_k^H = [\mathbf{\Lambda}_k \ \mathbf{0}_{M_B} \ \dots \ \mathbf{0}_{M_B}] \begin{bmatrix} \mathbf{H}_{w,0} \\ \mathbf{H}_{w,1} \\ \vdots \\ \mathbf{H}_{w,L-1} \end{bmatrix} \begin{bmatrix} \mathbf{H}_{w,0}^H & \mathbf{H}_{w,1}^H & \dots & \mathbf{H}_{w,L-1}^H \end{bmatrix} \begin{bmatrix} \mathbf{\Lambda}_k^H \\ \mathbf{0}_{M_B} \\ \vdots \\ \mathbf{0}_{M_B} \end{bmatrix} = \mathbf{\Lambda}_k \mathbf{H}_{w,0} \mathbf{H}_{w,0}^H \mathbf{\Lambda}_k^H.$$

For the sake of simplicity, in the following, we set $\mathbf{H}_{w,0} = \mathbf{H}_w$. The final expression for the uplink capacity distribution is given by

$$C \sim \frac{1}{N} \sum_{k=0}^{N-1} \log \left[\det \left(\mathbf{I}_{M_B} + \rho \mathbf{\Lambda}_k \mathbf{H}_w \mathbf{H}_w^H \mathbf{\Lambda}_k^H \right) \right]. \quad (20)$$

This result has two interesting interpretations. First, it says that only a small fraction of the total number of degrees of freedom in the i.i.d. gaussian matrix \mathbf{H} is contributing to capacity, which provides some insight into the relation between frequency-diversity and capacity. Second, it follows from (20) that the capacity of the delay spread channel is given by the sum of the capacities of N i.i.d. gaussian $M_B \times M_S$ channels followed by a frequency-dependent attenuation at each receive antenna (see Fig. 4). Note, however, that the N spatial channels contributing to capacity are fully correlated since they are all derived from the same i.i.d. gaussian matrix \mathbf{H}_w . A more detailed discussion of these observations is beyond the scope of this paper and will be reported elsewhere.

Downlink capacity. In the downlink case starting from (8) with $\gamma_0 = 0$ and using similar developments as in the uplink case, the capacity distribution is obtained as

$$C \sim \frac{1}{N} \sum_{k=0}^{N-1} \log \left[\det \left(\mathbf{I}_{M_S} + \rho \mathbf{H}_w^H \mathbf{\Lambda}_k^H \mathbf{\Lambda}_k \mathbf{H}_w \right) \right], \quad (21)$$

where \mathbf{H}_w and $\mathbf{\Lambda}_k$ have been defined above. Next, using the fact that

$$\det \left(\mathbf{I}_{M_S} + \rho \mathbf{H}_w^H \mathbf{\Lambda}_k^H \mathbf{\Lambda}_k \mathbf{H}_w \right) = \det \left(\mathbf{I}_{M_B} + \rho \mathbf{\Lambda}_k \mathbf{H}_w \mathbf{H}_w^H \mathbf{\Lambda}_k^H \right),$$

it follows that the distribution of downlink capacity is given by

$$C \sim \frac{1}{N} \sum_{k=0}^{N-1} \log \left[\det \left(\mathbf{I}_{M_B} + \rho \mathbf{\Lambda}_k \mathbf{H}_w \mathbf{H}_w^H \mathbf{\Lambda}_k^H \right) \right],$$

which proves the equivalence of the uplink and downlink capacity distribution. In the sequel, we shall therefore not distinguish between uplink and downlink capacity.

Bounds on capacity. In the following we shall derive bounds on expected capacity and the capacity distribution, which can be used to conveniently check the influence of physical parameters and system parameters on capacity without performing Monte-Carlo simulations. Let us first provide an upper bound on expected capacity. Starting from (20) we get

$$\mathcal{E}\{C\} = \frac{1}{N} \sum_{k=0}^{N-1} \mathcal{E} \left\{ \log \left[\det \left(\mathbf{I}_{M_B} + \rho \mathbf{\Lambda}_k \mathbf{H}_w \mathbf{H}_w^H \mathbf{\Lambda}_k^H \right) \right] \right\},$$

which noting that the function $\log \det$ is concave on the set of positive definite matrices [26] and applying Jensen's inequality [26] yields

$$\mathcal{E}\{C\} \leq \frac{1}{N} \sum_{k=0}^{N-1} \log \left[\det \left(\mathbf{I}_{M_B} + \rho \mathbf{\Lambda}_k \mathcal{E} \{ \mathbf{H}_w \mathbf{H}_w^H \} \mathbf{\Lambda}_k^H \right) \right],$$

and therefore

$$\mathcal{E}\{C\} \leq \frac{1}{N} \sum_{k=0}^{N-1} \sum_{i=0}^{r_k-1} \log \left(1 + \rho M_S |\lambda_{k,i}|^2 \right), \quad (22)$$

where r_k denotes the rank of $\mathbf{\Lambda}_k$ (or equivalently the number of nonzero entries). Here we have used $\mathcal{E}\{\mathbf{H}_w \mathbf{H}_w^H\} = M_S \mathbf{I}_{M_B}$, which follows from the fact that the elements on the main diagonal of $\mathbf{H}_w \mathbf{H}_w^H$ given by $y = \sum_{i=0}^{M_S-1} |y_i|^2$ with i.i.d. $y_i \sim \mathcal{CN}(0, 1)$ are chi-squared distributed with M_S degrees of freedom. Eq. (22) shows that the expected capacity is upper-bounded by the (normalized) sum of the capacities of N spatial subchannels $k = 0, 1, \dots, N - 1$, which themselves consist of r_k parallel scalar subchannels with power gain $M_S |\lambda_{k,i}|^2$.

We shall next derive the distribution of lower and upper bounds on (14). The techniques used below have mostly been borrowed from [7], especially the idea of using the QR-decomposition of the white channel transfer matrix \mathbf{H}_w in this context is taken from [7]. In the following we assume that $M_S \geq M_B$. With the QR-decomposition of the $M_S \times M_B$ matrix \mathbf{H}_w^H given by $\mathbf{H}_w^H = \mathbf{Q} \mathbf{R}_w$, we obtain from (21)

$$C \sim \frac{1}{N} \sum_{k=0}^{N-1} \log \left[\det \left(\mathbf{I}_{M_S} + \rho \mathbf{R}_w \mathbf{\Lambda}_k^H \mathbf{\Lambda}_k \mathbf{R}_w^H \right) \right].$$

Furthermore, since for any upper-triangular matrix \mathbf{R} [27]

$$\det(\mathbf{I} + \mathbf{R} \mathbf{R}^H) \geq \prod_l (1 + |r_{l,l}|^2),$$

where $r_{l,l}$ denotes the entries on the main diagonal of \mathbf{R} , we get the distribution of a capacity lower bound C_l as

$$C_l \sim \frac{1}{N} \sum_{k=0}^{N-1} \sum_{l=0}^{r_k-1} \log \left(1 + \rho |\lambda_{k,l}|^2 |r_{l,l}|^2 \right). \quad (23)$$

Similarly, using Hadamard's inequality [26] which states that for any nonnegative definite matrix \mathbf{H} , $\det(\mathbf{H}) \leq \prod_l h_{l,l}$, we can derive the distribution of a capacity upper bound C_u as

$$C_u \sim \frac{1}{N} \sum_{k=0}^{N-1} \sum_{l=0}^{r_k-1} \log \left[1 + \rho \left(|\lambda_{k,l}|^2 |r_{l,l}|^2 + \sum_{m=l+1}^{r_k-1} |\lambda_{k,m}|^2 |r_{l,m}|^2 \right) \right]. \quad (24)$$

Now, since the $|r_{l,l}|^2$ are independent and chi-squared distributed with $M_S - l$ degrees of freedom [28] it follows that the capacity of the delay-spread channel is lower bounded by the sum of the capacities of $\sum_{k=0}^{N-1} r_k$ subchannels, whose power gains consist of a deterministic factor $|\lambda_{k,l}|^2$ and a stochastic factor given by independent chi-squared random variables with degrees of freedom $M_S, M_S - 1, \dots, M_S - r_k + 1$ for $k = 0, 1, \dots, N - 1$. Since the off-diagonal entries of \mathbf{R}_w are i.i.d. $\mathcal{CN}(0, 1)$, a similar interpretation can be given for the upper bound.

4.4 The line-of-sight case

In the LOS-case, i.e., $\gamma_0 > 0$ the capacity has to be estimated directly from (14), since no further

analytical simplifications are possible. As we shall see in Simulation Example 5, a LOS-component in the channel in general reduces the capacity of an OFDM-based spatial multiplexing system.

5 Simulation Results

In this section, building on the results in Sec. 4, we describe a Monte-Carlo method for computing the expected capacity, outage capacity, and capacity cdf of OFDM-based spatial multiplexing systems, and we provide a number of simulation examples. In particular, we study the influence of the propagation environment and system parameters on capacity.

5.1 General Remarks on the Simulation Results

Based on (20) we can estimate the capacity distribution (and hence expected capacity, outage capacity, and the capacity cdf) using a Monte Carlo method. In each Monte Carlo run an $M_B \times M_S$ i.i.d. gaussian matrix \mathbf{H}_w is generated and the corresponding capacity C is computed according to (20). The resulting independent draws of the capacity random variable can then be used to estimate expected capacity, outage capacity, and the capacity cdf. Outage capacity is an important measure for channel capacity in quasi-static fading environments. Specifically, an outage capacity of C_q states that the channel capacity is less than C_q with probability q , i.e., $\text{Prob}[C > C_q] = 1 - q$. In our simulations we shall consider the case $q = 0.1$. In every simulation example 1,000 realizations of the matrix \mathbf{H}_w were used. Unless specified otherwise, the power delay profile was taken to be exponential, the OFDM-system parameters were chosen to be $N = 512, M = 576$, the relative antenna spacing was $\Delta = 0.5$, the LOS-component was set to $\gamma_0 = 0$, and a gaussian distribution was assumed for the angles of arrival. Finally, in the following SNR is defined as $\text{SNR} = M_T \rho = \frac{P}{N\sigma_n^2}$.

5.2 Simulation Results

Simulation Example 1. In the first simulation example, we study the impact of delay spread on channel capacity. The number of antennas was $M_B = M_S = 4$. The mean angles of arrival were drawn from a gaussian distribution with mean $\frac{\pi}{2}$ and variance $\frac{\pi}{170}$ and the angular spreads were drawn from a gaussian distribution with mean 0 and variance $\frac{\pi}{60}$. The actual realizations satisfied $\bar{\theta}_l \in [\frac{\pi}{3}, \frac{2\pi}{3}]$ and $\sigma_{\theta,l} \in [0, \frac{\pi}{4}]$. Note that the mean angles of arrival and the angular spreads were drawn only once for the entire simulation. More specifically, we fixed $\bar{\theta}_l$ and $\sigma_{\theta,l}$ for $l = 0, 1, \dots, 49$

and generated the spatial channels with different delay spreads by taking the first L parameter tuples $\{\bar{\theta}_l, \sigma_{\theta,l}\}$ from that specific draw. Fig. 5 shows the expected capacity and outage capacity (in bps/Hz) as a function of SNR for a delay spread of $L = 1, 5, 10, 20$ and 50 samples assuming that each sample corresponds to an independent scatterer. It is clearly seen that both the expected capacity and outage capacity increase for increasing channel delay spread, which corroborates the intuition that delay spread is a contributor to capacity.

Simulation Example 2. In this simulation example, we investigate the impact of angle spread and spread of mean angles of arrival on capacity. In both simulations the number of antennas was $M_B = M_S = 4$, the delay spread was assumed to be $L = 10$ and the SNR was 10dB. In the first example the mean angles of arrival were chosen as in Simulation Example 1 and the angular spreads were drawn from a gaussian distribution with mean 0 and variable variance. Fig. 6 shows the expected capacity as a function of $\max_l \sigma_{\theta_l}$. We can observe that the expected capacity increases for increasing angular spread up to a point where fading between the BTS antennas is uncorrelated. Increasing the angular spread beyond this point does not significantly increase capacity, since the correlation matrices \mathbf{R}_l already have full rank. For decreasing angular spread the expected capacity decreases up to a point where the correlation matrices \mathbf{R}_l have rank 1. Further decreasing the angular spread beyond this point does therefore not lead to a further decrease of expected capacity. In the second example, the impact of mean angle spread on expected capacity has been investigated. In this case the angular spread was chosen as in Simulation Example 1 and the mean angles of arrival were drawn from a gaussian distribution with mean $\frac{\pi}{2}$ and variable variance. Fig. 7 shows the expected capacity as a function of the mean angle spread. We can observe that the mean angle spread has the same qualitative influence on expected capacity as the angular spread of the individual scatterer clusters. Summarizing, environments with large angular spread or large mean angle spread yield increased capacity.

Simulation Example 3. In the third simulation example, we compare the capacity obtained using the stochastic parametric channel model proposed in [4, 8] with the capacity predicted by the space-time channel model proposed in this paper. In both cases we assumed that the delay spread is $L = 10$ and that each channel impulse response sample corresponds to an independent scatterer cluster. For the parametric channel model in each Monte Carlo run the angles of departure and the angles of arrival were drawn from two independent gaussian distributions with mean $\frac{\pi}{2}$ and variance $\frac{\pi}{170}$. Since the parameters for the space-time channel model were generated as in Simulation Example 1, this guarantees a fair comparison. For SNR = 20dB, Fig. 8 shows the expected capacity

(in bps/Hz) obtained from the two different channel models as a function of the number of antennas $M_B = M_S$. It is clearly seen that our space-time channel model predicts much higher capacities than the parametric channel model (see the comments in Sec. 2.4).

Simulation Example 4. In this simulation example, we investigate the influence of different assumptions on the statistics of the angles of arrival on capacity. For $M_B = M_S = 4$, and delay spread $L = 1, 10$ and 50 (same number of independent paths), we computed the expected capacity obtained by assuming a gaussian and a uniform distribution for the angles of arrival. For both case the mean angles of arrival were chosen as in Simulation Example 1. The angular spreads in the gaussian case were chosen as in Simulation Example 1, whereas in the uniform case we set $\delta_l = \sqrt{3}\sigma_{\theta_l}$ ($l = 0, 1, \dots, L - 1$), which guarantees that the variance of the angle of arrival in the uniform case is equal to the variance of the gaussian distributed angle of arrival. Fig. 9 shows the corresponding expected capacity. We can observe that for $L = 1$ and $L = 10$ the expected capacity is almost the same, whereas for $L = 50$ the gaussian assumption yields a slightly higher expected capacity.

Simulation Example 5. In this simulation example, we investigate the impact of a LOS-component on channel capacity. For $M_B = M_S = 4$ and channel parameters as in Simulation Example 1, Fig. 10 shows the expected capacity (in bps/Hz) at an SNR of 10dB for $L = 1, 5$ and 20 , respectively, as a function of the LOS-component γ_0 . In the case where only one scatterer cluster is present the LOS-component significantly reduces channel capacity, whereas in the cases $L = 5$ and $L = 20$ the capacity is basically unaffected by the LOS-component, which is due to the fact that in these cases there is only one Ricean fading scatterer cluster out of 5 and 20, respectively. The overall reduction in capacity is therefore negligible.

Simulation Example 6. In the last simulation example, we compute the complementary cdf (ccdf), and the expected capacity and outage capacity of spatial versions of the *hilly terrain* (HT), and *typical urban* (TU) power delay profiles taken from the GSM recommendations. The spatial fading statistics were chosen as in Simulation Example 1. For a bandwidth of 5MHz, in the TU case the delay spread is 25 samples and in the HT case it is 100 samples in accordance with the GSM recommendations. Furthermore, in the TU case the number of independent scatterer clusters is 12, whereas in the HT case it is 8. The OFDM system parameters were chosen to be $N = 512$ and $M = 640$. For $M_B = M_S = 4$, Fig. 11 shows the expected capacity and outage capacity of the TU channel as a function of SNR. Fig. 12 shows the capacity cdf for the TU channel at an SNR of 20dB for different numbers of antennas. The results for the HT case are very similar and will therefore

not be depicted. From the figures we can conclude that an OFDM-based spatial multiplexing system employing $M_B = M_S = 4$ antennas has an expected capacity of roughly 19bps/Hz at an SNR of 20dB in a TU environment. Taking into account the loss in spectral efficiency due to the CP this capacity corresponds to a data rate of approximately 70Mbps.

6 Conclusion

Based on an abstract model for stochastic spatial delay spread channels, we derived an expression for the capacity of OFDM-based spatial multiplexing systems. We provided a Monte-Carlo method for estimating the capacity cdf, expected capacity, and outage capacity, and we established bounds on capacity. We furthermore showed that the capacity of an OFDM-based spatial multiplexing system is equal to the sum of the capacities of N (fully correlated) spatial channels each of which consists of a white random channel followed by a frequency-dependent attenuation at each receive antenna.

Our simulation results show that delay spread and angle spread significantly boost the capacity of multi-antenna systems. For a spatial version of the typical urban channel proposed in the GSM recommendations and 4 transmit and 4 receive antennas, we found an expected capacity of roughly 19bps/Hz at an SNR of 20dB, which for a bandwidth of 5MHz results in a data rate of 70Mbps.

Directions for further work include the analysis of the case where there is scattering at both the transmitter and the receiver. A question of particular importance seems to be the analysis of the influence of scattering radiuses and distance between BTS and SU on capacity. Furthermore, a detailed study of the influence of different antenna geometries on the capacity of the delay spread channel appears to be of interest. This problem has been studied to some extent in [7] for the narrowband frequency-flat fading case. Finally, a thorough investigation of the effect of correlation between the different scatterer clusters on capacity seems to be worthwhile.

Acknowledgment

The authors would like to thank R. W. Heath Jr. for his comments on an earlier version of the paper.

References

- [1] A. J. Paulraj and T. Kailath, "Increasing capacity in wireless broadcast systems using distributed transmission/directional reception," *U. S. Patent*, no. 5,345,599, 1994.

- [2] G. J. Foschini, "Layered space-time architecture for wireless communication in a fading environment when using multi-element antennas," *Bell Labs Tech. J.*, pp. 41–59, Autumn 1996.
- [3] I. E. Telatar, "Capacity of multi-antenna gaussian channels," Tech. Rep. #BL0112170-950615-07TM, AT & T Bell Laboratories, 1995.
- [4] G. G. Raleigh and J. M. Cioffi, "Spatio-temporal coding for wireless communication," *IEEE Trans. Comm.*, vol. 46, no. 3, pp. 357–366, 1998.
- [5] G. J. Foschini and M. J. Gans, "On limits of wireless communications in a fading environment when using multiple antennas," *Wireless Personal Communications*, vol. 6, pp. 311–335, 1998.
- [6] T. L. Marzetta and B. M. Hochwald, "Capacity of a mobile multiple-antenna communication link in Rayleigh flat fading," *IEEE Trans. Inf. Theory*, vol. 45, pp. 139–157, Jan. 1999.
- [7] D. Shiu, G. J. Foschini, M. J. Gans, and J. M. Kahn, "Fading correlation and its effect on the capacity of multi-element antenna systems," *IEEE Trans. Comm.*, 1999. to appear.
- [8] G. G. Raleigh and V. K. Jones, "Multivariate modulation and coding for wireless communication," *IEEE J. Sel. Areas Comm.*, vol. 17, no. 5, pp. 851–866, 1999.
- [9] D. Asztély, "On antenna arrays in mobile communication systems: Fast fading and GSM base station receiver algorithms," Tech. Rep. IR-S3-SB-9611, Royal Institute of Technology, Stockholm, Sweden, March 1996.
- [10] J. Salz and J. H. Winters, "Effect of fading correlation on adaptive arrays in digital mobile radio," *IEEE Trans. Veh. Technol.*, vol. 43, no. 4, pp. 1049–1057, 1994.
- [11] A. F. Naguib, *Adaptive antennas for CDMA wireless networks*. Ph.D. dissertation, Department of Electrical Engineering, Stanford University, Aug. 1996.
- [12] J. Fuhl, A. F. Molisch, and E. Bonek, "Unified channel model for mobile radio systems with smart antennas," *IEE Proc.-Radar, Sonar Navig.*, vol. 145, pp. 32–41, Feb. 1998.
- [13] L. H. Brandenburg and A. D. Wyner, "Capacity of the gaussian channel with memory: The multivariate case," *Bell System Technical Journal*, vol. 53, pp. 745–778, May-June 1974.
- [14] R. S. Cheng and S. Verdú, "Gaussian multiaccess channels with ISI: Capacity region and multiuser water-filling," *IEEE Trans. Inf. Theory*, vol. 39, no. 3, pp. 773–785, 1993.
- [15] D. Agarwal, V. Tarokh, A. F. Naguib, and N. Seshadri, "Space-time coded OFDM for high data rate wireless communication over wideband channels," in *Proc. VTC 98*, pp. 2232–2236, May 1998.
- [16] Y. Li, N. Seshadri, and S. Ariyavisitakul, "Channel estimation for OFDM systems with transmitter diversity in mobile wireless channels," *IEEE J. Sel. Areas Comm.*, vol. 17, pp. 461–471, March 1999.
- [17] R. B. Ertel, P. Cardieri, K. W. Sowerby, T. S. Rappaport, and J. H. Reed, "Overview of spatial channel models for antenna array communication systems," *IEEE Personal Communications*, pp. 10–22, Feb. 1998.
- [18] R. W. Chang, "Synthesis of band-limited orthogonal signals for multi-channel data transmission," *Bell Syst. Tech. J.*, vol. 45, pp. 1775–1796, Dec. 1966.
- [19] A. Peled and A. Ruiz, "Frequency domain data transmission using reduced computational complexity algorithms," in *Proc. IEEE ICASSP-80*, (Denver, CO), pp. 964–967, 1980.
- [20] L. J. Cimini, "Analysis and simulation of a digital mobile channel using orthogonal frequency division multiplexing," *IEEE Trans. Comm.*, vol. 33, pp. 665–675, July 1985.
- [21] B. LeFloch, M. Alard, and C. Berrou, "Coded orthogonal frequency division multiplex," *Proc. of IEEE*, vol. 83, pp. 982–996, June 1995.
- [22] H. Sari, G. Karam, and I. Jeanclaude, "Transmission techniques for digital terrestrial TV broadcasting," *IEEE Communications Magazine*, pp. 100–109, Feb. 1995.
- [23] A. S. Macedo and E. S. Sousa, "Coded OFDM for broadband indoor wireless systems," in *Proc. IEEE Int. Conf. Communications (ICC)*, (Montreal (Canada)), 1997.
- [24] W. Hirt and J. L. Massey, "Capacity of the discrete-time gaussian channel with intersymbol interference," *IEEE Trans. Inf. Theory*, vol. 34, pp. 380–388, May 1988.

- [25] R. G. Gallager, *Information Theory and Reliable Communication*. Wiley, 1968.
- [26] T. M. Cover and J. A. Thomas, *Elements of Information Theory*. New York: Wiley, 1991.
- [27] R. A. Horn and C. R. Johnson, *Matrix Analysis*. New York: Cambridge Press, 1985.
- [28] R. J. Muirhead, *Aspects of Multivariate Statistical Theory*. Wiley, 1982.

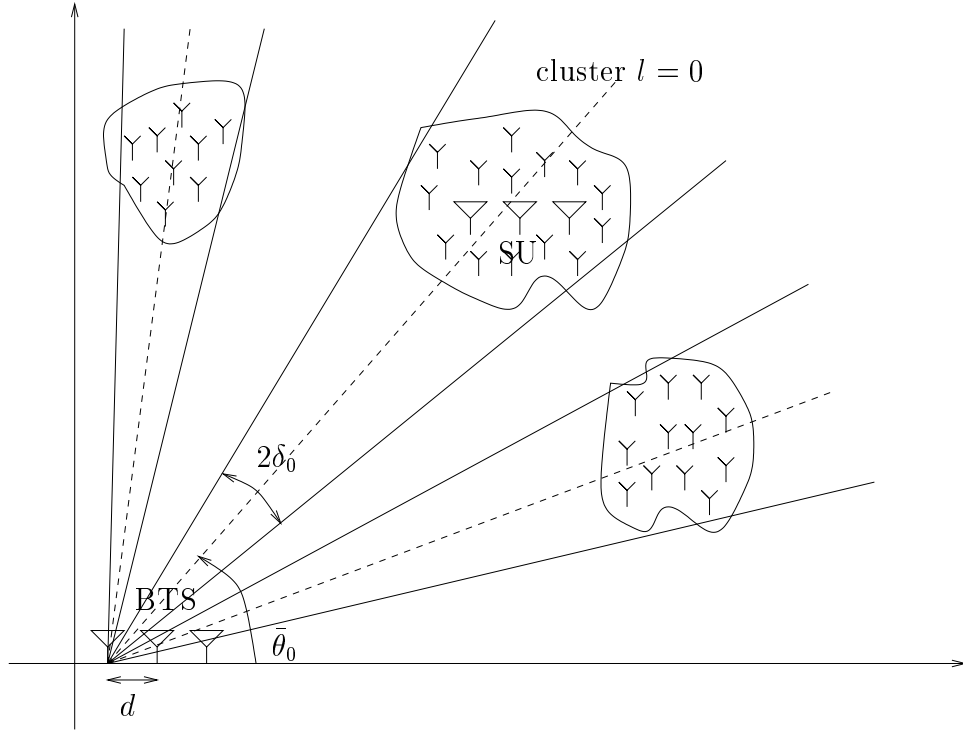


Fig. 1. Schematic representation of the space-time delay spread channel composed of multiple clustered paths. Each path cluster has a mean angle of arrival $\bar{\theta}_l$, an angle spread δ_l , and a delay τ_l .

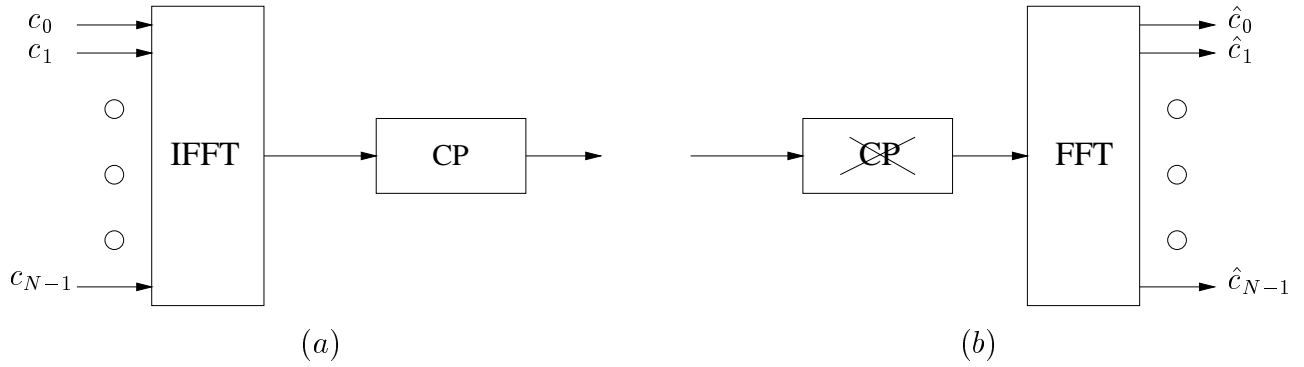


Fig. 2. Base-band OFDM transceiver: a) modulator, b) demodulator.

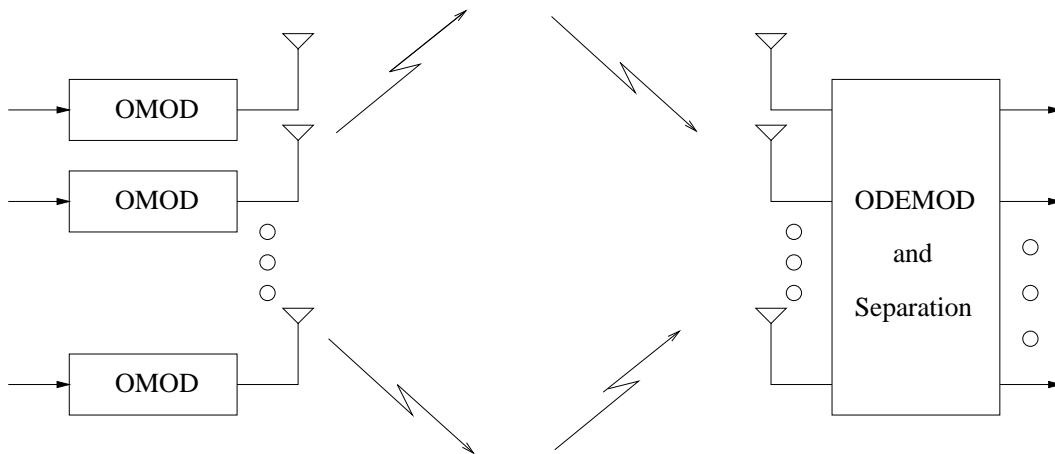


Fig. 3. OFDM-based spatial multiplexing system. (OMOD and ODEMOD denote an OFDM-modulator and demodulator, respectively.)

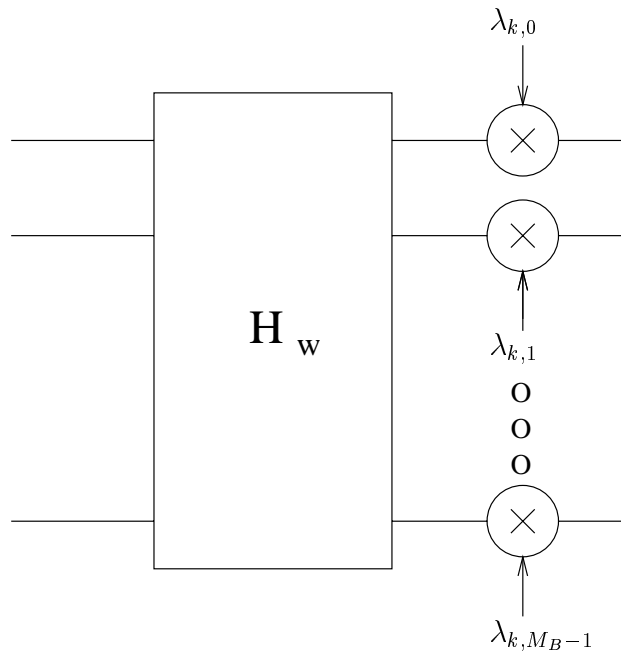


Fig. 4. Equivalent k -th tone subsystem.

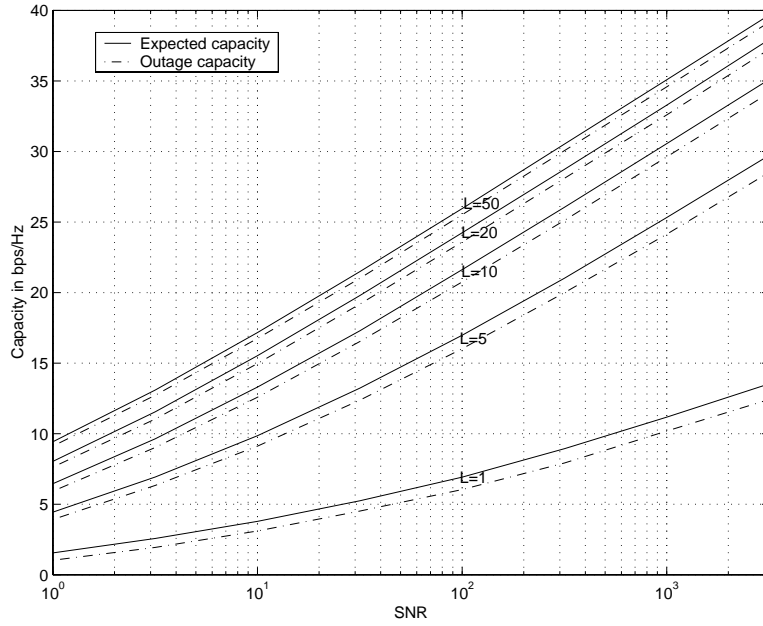


Fig. 5. Expected capacity and outage capacity in bps/Hz as a function of SNR for different channel delay spreads $L = 1, 5, 10, 20$ and 50 .

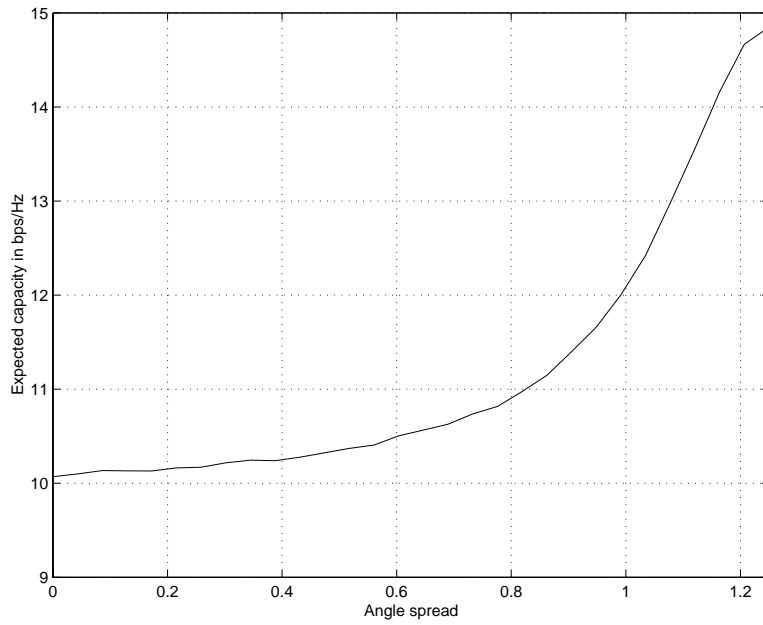


Fig. 6. Expected capacity in bps/Hz as a function of angle spread (i.e. $\max_l \sigma_{\theta_l} / \pi$) for $L = 10$ and $SNR = 10dB$.

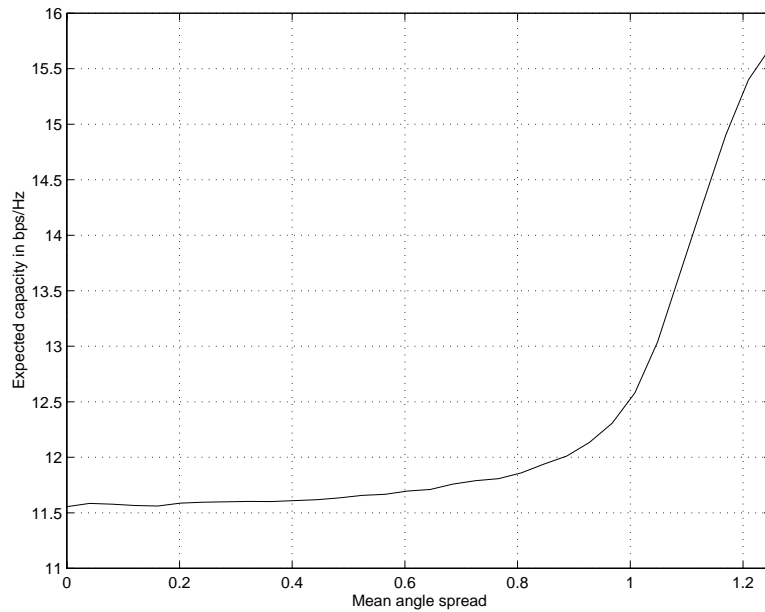


Fig. 7. Expected capacity in bps/Hz as a function of mean angle spread (normalized to π) for $L = 10$ and $SNR = 10dB$.

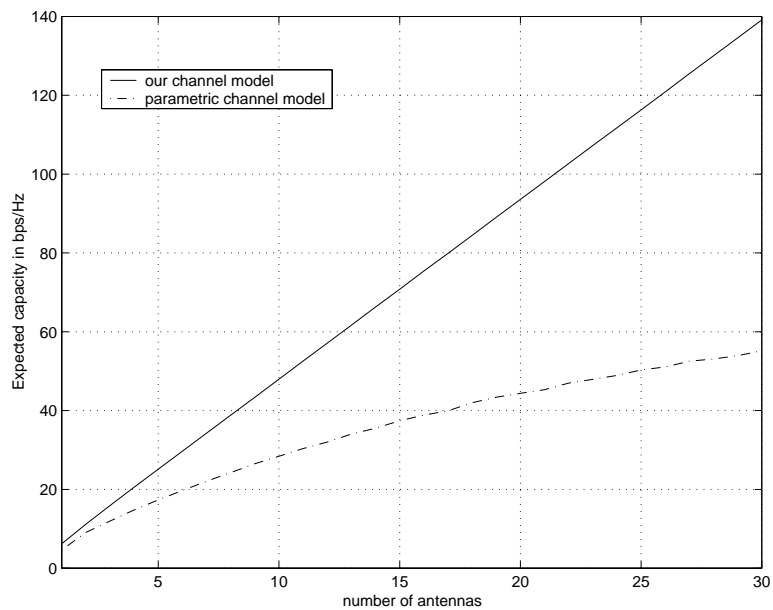


Fig. 8. Comparison of the capacity obtained using the parametric channel model from [4, 8] and the space-time channel model proposed in Sec. 2. The expected capacities are shown as a function of the number of antennas $M_B = M_S$.

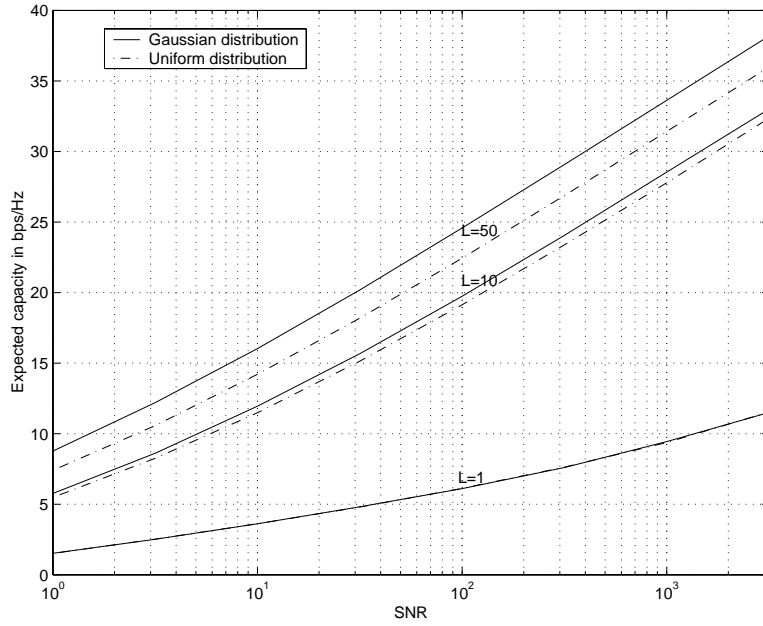


Fig. 9. Comparison of different assumptions on the statistics of the angles of arrival. For $L = 1, 10$ and 50 the expected capacity (in bps/Hz) is shown as a function of SNR for gaussian distributed and uniformly distributed angles of arrival.

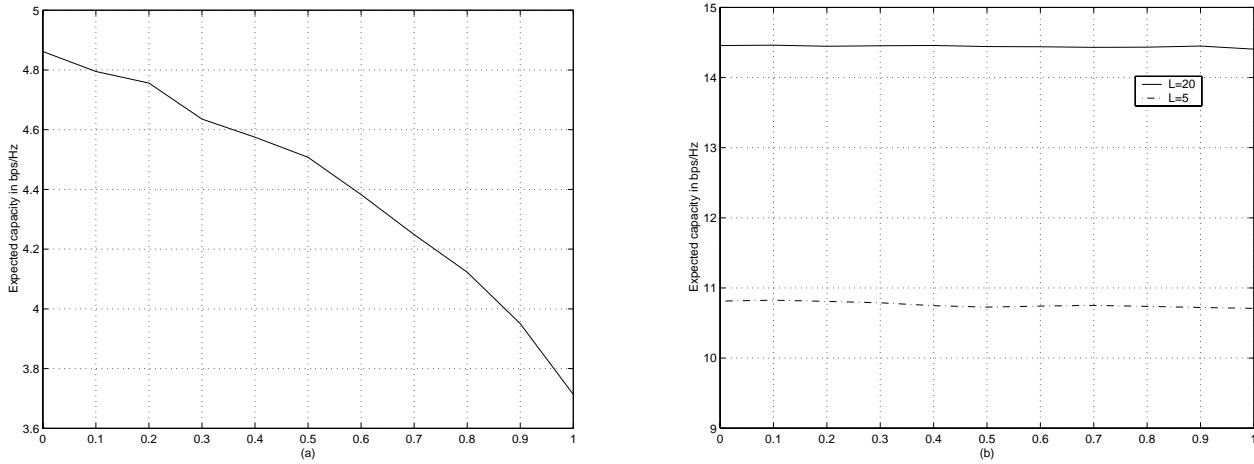


Fig. 10. Influence of a LOS-component on channel capacity. Expected capacity (in bps/Hz) as a function of γ_0 for a) $L = 1$, and b) $L = 5, 20$.

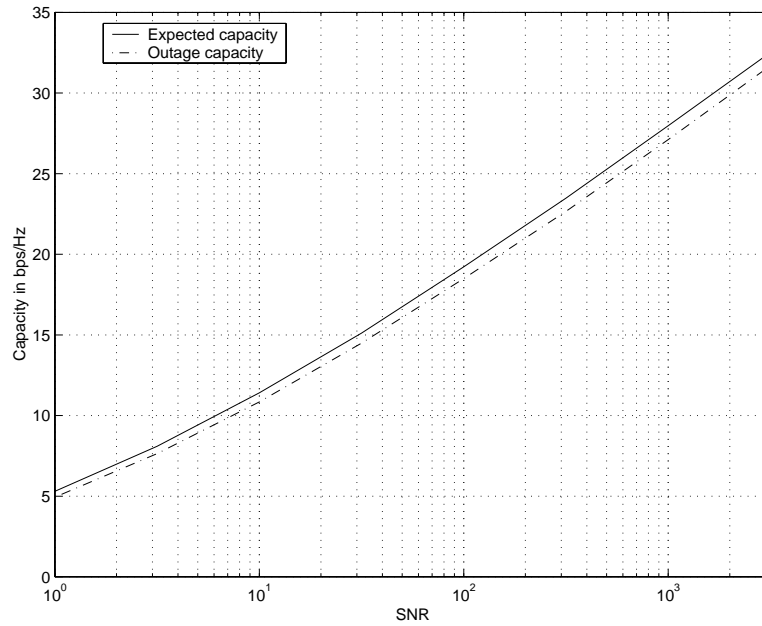


Fig. 11. Expected capacity and outage capacity for the power delay profile corresponding to the GSM typical urban channel model.

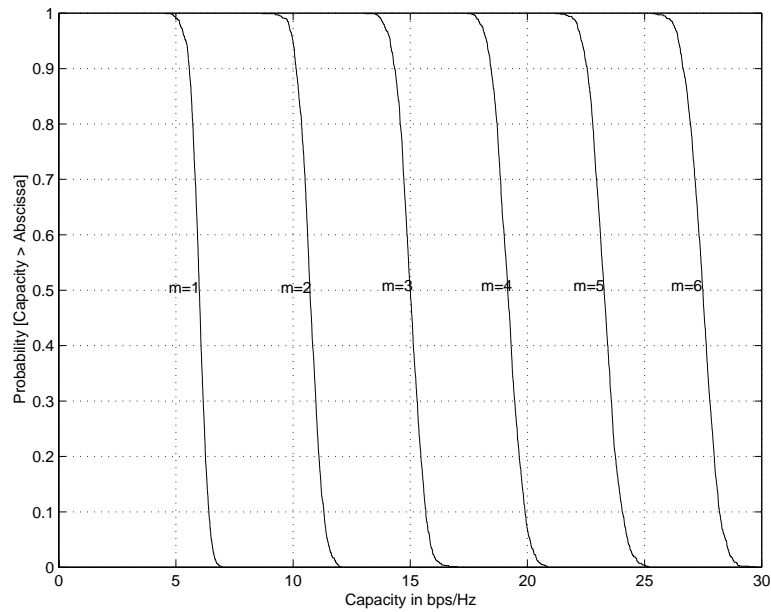


Fig. 12. Capacity cdfs for the GSM typical urban power delay profile at an SNR of 20dB for different numbers of antennas $m = M_B = M_S$.